Title

Investigation of immune cell markers in feline oral squamous cell carcinoma

Authors

Sparger, Ellen E

Murphy, Brian G

Kamal, Farina Mustaffa

et al.

Publication Date

2018-08-01

DOI

10.1016/j.vetimm.2018.06.011

Peer reviewed

Veterinary Immunology and Immunopathology 202 (2018) 52–62

Contents lists available at ScienceDirect

Veterinary Immunology and Immunopathology

journal homepage: www.elsevier.com/locate/vetimm

Research paper

Investigation of immune cell markers in feline oral squamous cell carcinoma

Ellen E. Sparger[a,*], Brian G. Murphy[b], Farina Mustaffa Kamal[a,1], Boaz Arzi[c], Diane Naydan[b], Chrisoula T. Skouritakis[c], Darren P. Cox[d,2], Katherine Skorupski[c]

[a] Department of Medicine and Epidemiology, School of Veterinary Medicine, University of California, Davis, CA, USA
[b] Department of Pathology, Microbiology, and Immunology, School of Veterinary Medicine, University of California, Davis, CA, USA
[c] Department of Surgical and Radiological Sciences, School of Veterinary Medicine, University of California, Davis, CA, USA
[d] Department of Orofacial Sciences, University of California, San Francisco, CA, USA

ARTICLE INFO

Keywords:
Feline oral cancer
Squamous cell carcinoma
Lymphoid cell infiltrates
Tregs
COX-2
Histologic subtypes

ABSTRACT

Squamous cell carcinoma is the most common oral cancer in the cat and presents as a locally aggressive lesion for which an effective therapeutic protocol remains elusive. Feline oral squamous cell carcinoma (OSCC) shares many clinical characteristics with human head and neck squamous cell carcinoma (HNSCC). Accordingly, present studies were conducted to determine similarities for immune markers shared by feline OSCC and human HNSCC. Biopsies harvested from a feline patient cohort-1 (n = 12) were analyzed for lymphoid cell infiltrates by immunohistochemistry (IHC). Results revealed unique patterns of T cell infiltration involving both neoplastic epithelium and stroma that were detected in most patient tumor biopsies (92%) examined by IHC staining for CD3. Intratumoral B cell infiltrates were detected within tumor stroma only, based on IHC staining for CD79a and CD20 for all patients within the same cohort-1. Infiltration of tumors by a regulatory CD4 T cell subset (Tregs) defined by expression of the forkhead transcription factor FoxP3, was also detected in biopsies from 57% of patients and involved infiltration of neoplastic epithelium and stroma. Patient biopsies were also examined for expression of immunomodulator cyclooxygenase (COX)-2 and revealed positive but weak staining of neoplastic epithelium in a significant proportion of cases (75%). Interestingly, COX-2 expression was detected in both neoplastic epithelium and stroma. Blood collected from a second cohort of feline OSCC patients (n = 9) revealed an increased frequency of circulating CD4 + FoxP3 + T cells when compared to healthy adult controls (n = 7) ($P = 0.045$), although frequencies of CD4 + CD25 + FoxP3 + T cells were comparable between patients and healthy pet cat controls. Lastly, biopsies from feline OSCC patients were characterized for histologic subtype using a classification scheme previously described for human HNSCC. This analysis revealed the conventional subtype as the predominant variant (75%) with conventional subtypes split evenly between well differentiated and moderately differentiated carcinomas. Two cases were classified as papillary and one case as basaloid subtypes. Correlations between subtype, immune marker scores or circulating Treg frequencies and clinical characteristics or outcome were not detected, most likely due to small patient numbers within patient cohorts. However, findings from these studies provide a preliminary step in the characterization of immune and histologic markers that will be critical to defining prognostic immune markers for feline OSCC and potential targets for testing of immunotherapeutics also relevant to human HNSCC in future studies.

1. Introduction

Squamous cell carcinoma is the most common oral tumor in the cat representing approximately 70% of tumors of the feline mouth (Wypij, 2013; Bilgic et al., 2015; Supsavhad et al., 2016). Feline oral squamous cell carcinoma (OSCC) is highly locally aggressive, often extending into bone and can be associated with pain, drooling, and inability to eat. Without treatment, OSCC leads to death or euthanasia within 4–8 weeks of diagnosis in most cats. The majority of cats present with tumors not amenable to surgical resection either due to tumor size or involvement of structures that cannot be fully resected such as the tongue. Furthermore, large surgical resections involving the jaw or tongue typically lead to non-recoverable anorexia in most feline patients. Studies have shown that radiation therapy and chemotherapy

* Corresponding author.
E-mail address: eesparger@ucdavis.edu (E.E. Sparger).
[1] Present address: Department of Veterinary Pathology and Microbiology, Universiti Putra Malaysia, Serdang, Selangor, Malaysia.
[2] Present address: Department of Diagnostic Services, School of Dentistry, University of Pacific, San Francisco, CA, USA.

https://doi.org/10.1016/j.vetimm.2018.06.011
Received 18 October 2017; Received in revised form 4 May 2018; Accepted 13 June 2018

are largely ineffective at prolonging life beyond 4–6 months. The etiology and pathogenesis of OSCC in the cat are poorly understood and investigation of dysregulated inflammatory and biochemical pathways potentially involved in malignant transformation has not been adequately pursued.

Human head and neck cancer represents 3–5% of human cancers in the United States and is the 7th most commonly diagnosed cancer worldwide. The vast majority of human head and neck cancers are oral squamous cell carcinomas with the oral cavity, oropharynx, and larynx as the most common sites for these cancers (Rettig and D'Souza, 2015). The most common causes for human head and neck squamous cell carcinoma (HNSCC) include prolonged exposure to tobacco and alcohol (Cooper et al., 2009; Rettig and D'Souza, 2015). Additionally, the incidence is increasing in the population under 40 years of age due to human papillomavirus (HPV) infections, particularly for those arising in the oropharynx (Rettig and D'Souza, 2015). Interestingly, a single feline OSCC sample assayed for felis catus papillomavirus (FcaPV) type 2 (FcaPV-2) was found positive for Fca-PV-2 RNA (Altamura et al., 2016). However, current findings that also include a cohort of 36 feline patients examined for FcaPV-1 and FcaPV-4 (Munday and French, 2015) do not yet support FcaPV as a significant etiology for feline OSCC. Most human HNSCC are locally invasive and demonstrate a high metastatic rate. Treatment consisting of surgery and chemo-radiation is effective as front-line intervention particularly for HPV-related cases, but those patients with recurrent or treatment refractory tumors have few effective therapeutic options (Cooper et al., 2009; Rettig and D'Souza, 2015). Research is ongoing to identify new therapeutic targets for patients with treatment-refractory human HNSCC.

Although studies both *in vitro* and *in vivo* using inbred immunodeficient mouse models often show efficacy in experimental studies, these findings often do not translate to efficacious treatment protocols for human cancers (Paoloni and Khanna, 2008; Gould et al., 2015). Consequently, recent attention has been directed to spontaneous models of cancer, particularly in pet dogs (Khanna et al., 2006; LeBlanc et al., 2016). Likewise, due to demonstrated similarities in biologic behavior between feline OSCC and treatment-refractory human HNSCC, the domestic cat may be a more predictive model of response to novel cancer therapies compared to mouse models (Wypij, 2013; Supsavhad et al., 2016).

Inflammation and immunosuppression have been repeatedly implicated in the processes of malignant transformation and tumor progression in human HNSCC (Feller et al., 2013). Related to this human cancer, an array of inflammatory and immunosuppressive cytokines and mediators have been shown to be dysregulated including cyclooxygenase-2 (COX-2), tumor necrosis factor (TNF)-α, interleukin (IL)-6, IL-1β, STAT3, and transforming growth factor (TGF)β1 (Feller et al., 2013; Ferris, 2015). COX-2 is another immune marker shown to be associated with epithelial cancers including human HNSCC and is typically induced by inflammation and stimuli associated with proliferation. COX-2 expression has been shown to correlate with tumor recurrence, metastasis, and response to therapy in people with advanced stage HNSCC (Feller et al., 2013; Yang et al., 2016). Tumor infiltrating T cell populations have also been shown to correlate with overall survival and response to therapy based on the identity of lymphocyte subsets involved (Ferris, 2015; Lei et al., 2016; De Meulenaere et al., 2017). Increased numbers of tumor infiltrating regulatory T cells (Tregs), an immunosuppressive CD4 T cell subset, have been often documented in tissue samples and in circulation in patients with human HNSCC (Allen et al., 2015; Ferris, 2015; Wallis et al., 2015). Tumor infiltrating Treg numbers have also been shown to correlate with prognosis in human patients with HNSCC although reports have often revealed conflicting results (Shang et al., 2015; Wallis et al., 2015; De Meulenaere et al., 2017). Ongoing investigations are focused on the identification of inflammatory and immunologic processes that may serve as potential therapeutic targets in human HNSCC, particularly given the recent successes of checkpoint inhibitors for specific human cancers (Lechner et al., 2017).

COX-2 expression has been examined in feline OSCC biopsies, although results have been inconsistent and have not correlated with clinical or inflammatory cell data (Hayes et al., 2006; DiBernardi et al., 2007; Millanta et al., 2016). However, associations between COX-2 expression and inflammation, as well as vascular endothelial growth factor (VEGF) expression, have been described for feline cutaneous squamous cell carcinomas (Bardagi et al., 2012; Millanta et al., 2016). Taken as a whole, little information is available relating to immunomodulatory factors and immune cell infiltrates associated with feline OSCC. Therefore, goals of this current study included investigation of lymphoid cell infiltrates and COX-2 expression in biopsies harvested from one feline OSCC patient cohort, and also an examination for frequencies of circulating Tregs in a second feline patient cohort. One overall aim for these investigations was to determine similarities in immune profiles shared between feline OSCC and human HNSCC, which may in turn inform immune correlates for disease outcome and future testing of immunotherapeutics for feline OSCC. A second aim of this investigation was to characterize feline OSCC according to histologic subtypes based on a classification scheme previously described for human HNSCC (Barnes et al., 2005) to further characterize similarities shared between the feline and human versions of this oral cancer. Accordingly, OSCC subtype classification provides another biological parameter that may be examined as a prognostic correlate for clinical outcome in future investigations of this feline cancer.

2. Materials and methods

2.1. Sample acquisition

Formalin-fixed, paraffin-embedded (FFPE) tumor tissue samples from feline OSCC cases were obtained through a search of the pathology database of the University of California, Davis (UC Davis) Veterinary Medical Teaching Hospital (VMTH). Additional FFPE tumor tissue samples were obtained from a previously published study (Skorupski et al., 2011). Whole blood samples were collected from feline OSCC patients presenting to the VMTH, healthy VMTH employee pets, and from a colony of adult specific pathogen free (SPF) bred cats housed at the breeding colony of the Feline Nutrition and Pet Care Center, School of Veterinary Medicine, UC Davis. Collection of peripheral blood from healthy adult SPF cats was conducted according to regulations and guidelines of the UC Davis Institutional Animal Care and Use Committee (IACUC protocol #15309). UC Davis has an Animal Welfare Assurance on file with the National Institutes of Health Office of Laboratory Animal Welfare (OLAW), and is fully accredited by the Association for the Assessment and Accreditation of Laboratory Animal Care, International (AAALAC). All blood samples from feline patients and healthy pet cats (adult non-SPF controls) were taken with informed owner consent with approval from the UC Davis Clinical Trials Review Board also governed by the UC Davis Institutional Animal Care and Use Committee.

2.2. Histologic review and classification

All tissues were fixed in 10% buffered formalin for at least 48 h prior to processing. Samples including mineralized bony tissue underwent decalcification using 15% formic acid prior to routine tissue processing. Five μm thick sections from formalin-fixed and paraffin-embedded tissues were stained with haematoxylin and eosin (HE) and assessed histologically by a veterinary pathologist (B.G.M). Organization of selected feline OSCC cases according to histological subtypes was based upon a classification scheme previously described for human HNSCC and canine OSCC (Barnes et al., 2005; Nemec et al., 2012). This scheme for classification was applied to feline OSCC lesions within this study by a board certified veterinary pathologist and human oral maxillofacial pathologist (B.G.M. and D.P.C., respectively).

2.3. Immunohistochemistry

Immunohistochemistry (IHC) staining was performed on serial 4 µm sections using a routine streptavidin–biotin horseradish peroxidase (HRP) detection system as previously described (Arzi et al., 2011). Briefly, the slides were deparaffinised and gradually hydrated to 70% ethanol. Endogenous peroxidase activity was blocked with immersion in H_2O_2 0.03% in methanol for 30 min. Antigen retrieval for slides stained with FOX-P3, CD79a, CD20, CD3, and COX-2 was accomplished *via* steam heat treatment with citrate (Dako Products Agilent; Santa Clara CA) for 30 min prior to cooling for 10 min. For staining of cytokeratins, sections were immersed in proteinase-K (Dako Products Agilent) for 7 min at room temperature (RT).

After pre-treating, non-specific antibody interactions were then blocked by immersion in 10% normal horse serum for 20 min. Primary antibodies included mouse monoclonal anti-CD79a (1:30 dilution, clone HM57; Dako Products Agilent), anti-pan-cytokeratin (1:600, clone Lu5; Biocare Medical; Pacheco CA), anti-COX-2 (1:100 dilution; clone 33; BD Biosciences; San Jose CA); rabbit polyclonal anti-CD20 (1:100, NeoMarker RB-9013-P1; Thermo Fisher Scientific; Waltham MA); and rat monoclonal anti-FoxP3 (10 µg/ml; clone FJK-16 s; eBioscience; Waltham MA) and anti-CD3 (1:10, clone CD3-12; Bio-Rad Antibodies-Serotec; Hercules CA). Slides were drained and primary antibodies were applied one hour and 30 min at RT for all remaining antibodies.

Biotinylated anti-rat secondary antibody (Biocare Medical) and streptavidin–HRP were applied to FoxP3 and CD3 antibody-stained slides according to the manufacturer's instructions (Biocare Medical). For mouse monoclonal antibodies to CD79a and pan-cytokeratin and rabbit polyclonal anti-CD20, biotinylated anti-mouse and anti-rabbit secondary antibodies (Biocare Medical) were applied according to the manufacturer's instructions. For COX-2 staining, HRP-labeled polymer anti-mouse IgG (EnVision K4001, Dako Products) was applied for 60 min RT. Positive labelling was visualized using 3-amino-9-ethycarbazole (AEC) (Invitrogen, Waltham MA) as the chromogen. Slides were counterstained with Mayer's haematoxylin (Millipore Sigma, St. Louis MO). Negative controls were prepared by omitting the primary antibody while including labelled secondary antibody. A semi-quantitative scoring scheme based upon the average density of positive-staining cells for the section was utilized for assessment of expression of each immune marker. Staining was scored based on the number of positive-staining cells per 400x field with 1–5 cells designated as 1+, 6–30 cells as 2+, > 30 cells as 3+ and no positive-staining cells as 0. To establish the average density of positive-staining cells, each section was first examined and scanned at low power magnification before switching to 400× magnification. Biopsies were scored for staining for each marker by a board-certified veterinary pathologist (B.G.M.)

2.4. Flow cytometry

Peripheral blood mononuclear cells (PBMC) were isolated from feline blood samples by density centrifugation using Ficoll-Histopaque (SigmaMillapore). A minimum of 2×10^6 cells were characterized for Treg frequency by first surface staining with Pacific Blue®-conjugated anti-feline CD4 clone 34F4 (Molecular Probes Inc., Waltham MA and Southern Biotech, Birmingham AL), and FITC-conjugated anti-feline CD25 clone 9F23 (courtesy of K. Ohno; University of Tokyo, Tokyo Japan). Surface staining for CD8 was also performed with PE-Cy7 or PE-conjugated anti-feline CD8 clone vpg-9 (Bio-Rad Antibodies-Serotec). Intracellular staining was performed using a commercial kit (FoxP3 Staining Kit; eBioscience) with PE, PE-Cy7 or Alexa Fluor® 647-conjugated anti-human CD3 clone CD3-12 (Bio-Rad Antibodies-Serotec) (Moore et al., 2005, 2012) and Alexa Fluor® 700 conjugated anti-mouse/rat FoxP3 clone FJK16 s (eBioscience). Cells were assessed for viability using Live/Dead® Fixable Aqua stain (Invitrogen). Controls included fluorescence minus one (FMO) staining for each antibody and PBMC activated with mitogen concanavalin-A as biological controls. Compensation settings were accomplished using BD CompBeads (BD Biosciences). Data were acquired using an LSRII flow cytometer (BD Biosciences) and 200,000 events were obtained for each sample and analyzed using FlowJo software (TreeStar, Inc., Ashland OR).

2.5. Statistical analysis

Statistical analysis and graphing were performed using GraphPad Prism (GraphPad Software, Inc., San Diego CA). An unpaired *t*-test was used to compare ages between different groups of cats. Correlation analyses were performed by Spearman's rank tests. Pair-wise analysis was performed to compare median frequencies of CD4 T cell subsets between patient and control cat groups using the Mann-Whitney U test (one-tailed). P values < 0.05 were considered significant.

3. Results

3.1. Patient description

Immunohistochemical studies were conducted on tumor tissues obtained from twelve cats (cohort-1) diagnosed with OSCC that included eight spayed females and four neutered males (Table 1). Age was unknown for one cat, but the mean age of remaining cats was 9.5 years (median 8 years, range of 4–15). Breeds within this cohort-1 included seven domestic shorthairs, four domestic longhairs, and one Burmese cat. Flow cytometry was performed on PBMC isolated from blood samples collected from a second cohort of nine cats with OSCC and eleven healthy control cats that included both client-owned and colony SPF cats. Cats within this second OSCC cohort (cohort-2) were characterized by a mean age of 12 years (median 12.5; range, 6–17 years), whereas a mean age of 9 years (median 10; range, 5–14 years) was determined for control cats (Table 2). Cats presenting with feline OSCC within this cohort-2 were significantly older than control cats ($P = 0.02$). Six control pet cats demonstrated mild to moderate periodontal disease at the time of sampling and one pet cat demonstrated severe focal periodontitis. Normal oral examinations were recorded for the four SPF control cats.

3.2. Histological classification according to OSCC subtype

Tumor anatomic locations of the feline OSCC case cohort-1 are provided in Table 1. Tumor sites were hard palate/maxilla (n = 8), mandible (n = 3) and tongue (n = 1). Review of feline cases within this study revealed OSCC subtypes that included conventional OSCC (n = 9; 75%) further characterized as either well differentiated (n = 4) or moderately differentiated (n = 5), papillary OSCC (n = 2; 16.7%), or

Table 1
Clinical characteristics of cohort-1 cats with tumors evaluated in immunohistochemical studies.

Case #	Tumor Site	Age (years)	Sex	Breed	Weight (kg)
Case 1	R Mandible	14	FS	DSH	3.4
Case 2	R Mandible	12	MN	DLH	4.6
Case 3	R Maxilla	15	FS	DSH	3.1
Case 4	R Maxilla	6	MN	DLH	4.2
Case 5	R Maxilla	14	FS	DLH	5.1
Case 6	Tongue Base	8	MN	DLH	4.8
Case 7	R Maxilla	12	FS	DSH	3.1
Case 8	L Maxilla	8	FS	Burmese	3.1
Case 9	R Maxilla	7	FS	DSH	3.2
Case 10	R Maxilla	U	FS	DSH	5.4
Case 11	L Maxilla	4	FS	DSH	2.3
Case 12	R Mandible	5	MN	DSH	4.5

R = right side; L = left side; DSH = Domestic shorthair; DLH = Domestic longhair; FS = female, spayed; MN = male, neutered; U = unknown.

Table 2
Clinical characteristics of cohort-2 cats evaluated for circulating Treg frequencies.

Case #	Diagnosis	Tumor Site	Age (years)	Sex	Breed	Weight (kg)
Case 13	SCC	R Mandible	12	MN	DLH	4.9
Case 14	SCC	Tongue Base	13	MN	DLH	4.7
Case 15	SCC	L Maxilla	8	FS	DSH	4.5
Case 16	SCC	R Maxilla	16	MN	DSH	7.0
Case 17	SCC	Tongue Base	13	FS	Maine Coon	U
Case 18	SCC	Tonsil	9	MN	DSH	6.9
Case 19	SCC	L Maxilla	14	MN	Bombay	3.8
Case 20	SCC	R Mandible	14	MN	DSH	8.7
Case 21	SCC	R Mandible	12	MN	DSH	5.6
Control 1	Adult Non-SPF	n/a	5	FS	DSH	3.8
Control 2	Adult Non-SPF	n/a	5	MN	DSH	7.3
Control 3	Adult Non-SPF	n/a	5	MN	DSH	6.5
Control 4	Adult Non-SPF	n/a	7	MN	DSH	6.0
Control 5	Adult Non-SPF	n/a	8	FS	DLH	5.5
Control 6	Adult Non-SPF	n/a	14	FS	DSH	2.5
Control 7	Adult Non-SPF	n/a	13	FS	DSH	4.0
Control 8	Adult SPF	n/a	10	M	DSH	U
Control 9	Adult SPF	n/a	10	M	DSH	U
Control 10	Adult SPF	n/a	11	F	DSH	U
Control 11	Adult SPF	n/a	11	F	DSH	U

R = right side; L = left side; DSH = Domestic shorthair; DLH = Domestic longhair; FS = female, spayed; MN = male, neutered; SPF = specific pathogen free; U = unknown; n/a = not applicable.

Table 3
Histologic subtype and immune marker analysis of feline OSCC cohort-1.

Case #	SCC Subtype	COX-2	CD3	FoxP3	CD79a	CD20
Case 1	Conventional WD	1+	1+	1+	1+	ND
Case 2	Conventional WD	1+	2+	0	3+	ND
Case 3	Papillary WD	1+	2+	0	1+	2+
Case 4	Conventional MD	2+	3+	1+	2+	2+
Case 5	Conventional MD	0	2+	1+	3+	3+
Case 6	Basaloid	1+	3+	2+	2+	2+
Case 7	Conventional MD	1+	2+	1+	1+	1+
Case 8	Conventional WD	1+	1+	0	1+	1+
Case 9	Papillary WD	0	3+	2+	3+	3+
Case 10	Conventional MD	0	0	0	1+	ND
Case 11	Conventional WD	1+	1+	1+	1+	ND
Case 12	Conventional MD	1+	1+	0	1+	ND
Control	Not applicable	0	0	0	0	0

WD and MD represent well differentiated and moderately differentiated respectively. Scores are based on frequency of cell numbers per high power field as described in Methods. ND represents not determined.

basaloid OSCC (n = 1; 8.3%) (Table 3), based on a classification scheme described for human HNSCC and canine OSCC (Barnes et al., 2005; Nemec et al., 2012).

Tumors identified as conventional, well-differentiated OSCC resembled normal squamous epithelium with a generally orderly progression towards keratinization (Nemec et al., 2012) as shown in a representative example (case 11) in Fig. 1A. Intraepithelial central aggregates of keratin (keratin pearls) were common in conventional, well-differentiated OSCC lesions. Conventional, moderately differentiated tumors demonstrated distinct nuclear pleomorphism, and increased mitotic activity while epithelial keratinization was less pronounced. A representative example of a papillary OSCC subtype (case 9; Fig. 1B) featured a papillary growth pattern organized around thin cores of fibrovascular stroma. An example of basaloid SCC (case 6; Fig. 1C) demonstrated a predominance of closely packed small to medium sized basophilic epithelial cells associated with fewer eosinophilic keratinocytes. The diagnosis of OSCC required the identification of epithelial invasion through the basement membrane into the subjacent stroma. Such invasion is highlighted by cytokeratin staining by IHC as shown in Fig. 1D (case 1).

3.3. IHC analysis of immunologic markers

Biopsies from twelve feline OSCC patients (cohort-1; Table 1) were analyzed by IHC for specific immune cell markers using a semi-quantitative scoring system with findings summarized in Table 3. T cell infiltrates as determined by positive cytoplasmic staining for CD3, were detected in biopsies for eleven of the twelve (92%) patients within cohort-1. Scores for T cell infiltrates were evenly distributed in magnitude across cases with four cases scored as either 1+ or 2+, and three cases scored as 3+ (Table 3). Two phenotypes of T cell infiltrates were observed with one phenotype characterized by CD3+ cells distributed within the tumor stroma (fibrovascular connective tissue) and neoplastic epithelium for seven of the patient biopsies (cases 1–6, 8) with a representative example (case 4) shown in Fig. 2A. A second phenotype detected in four cases (cases 7, 9, 11–12) revealed CD3+ cells predominantly within the tumor stromal with few or minimal T cells observed within neoplastic epithelium as demonstrated in Fig. 2B (case 9).

B cell infiltrates for all twelve cases were assessed by staining for CD79a, a component of the B cell antigen receptor, and were detected in all twelve case biopsies (Table 3). The most frequent findings (7/12 cases) were characterized as rare B cells detected within tumor stroma and associated with a score of 1 + . However, a subset of cases (5/12) revealed significant B cell infiltrates scored as either 2+ or 3+ and demonstrated moderate to large numbers of B cells within the tumor stroma as shown for representative cases in Fig. 2C (case 9) and 2D (case 2). Furthermore, two cases (cases 8–9) revealed B cell follicle-like structures (lymphoid follicles) within the tumor stroma with a representative case shown in Fig. 2C (case 9). Of note, a correlation analysis revealed a significant association between CD3 and CD79a IHC scores ($r = 0.708$; $P = 0.012$).

A subset of cohort-1 case biopsies (7/12) were also scored for B cell infiltrates by staining for B lymphocyte antigen CD20 in addition to staining for CD79 A. Of note, CD79a staining is typically also associated with weak background staining of tissue fibroblasts, which must be distinguished from specific staining of tissue B cells. B cell infiltrate scores and staining based on CD79a and CD20 expression were compared in Table 3 and Fig. 3A–B (case 9) and Fig. 3C–D (case 5) and revealed comparable scores for those cases examined with both B cell marker antibodies.

Examination for infiltration of Tregs was performed by staining for

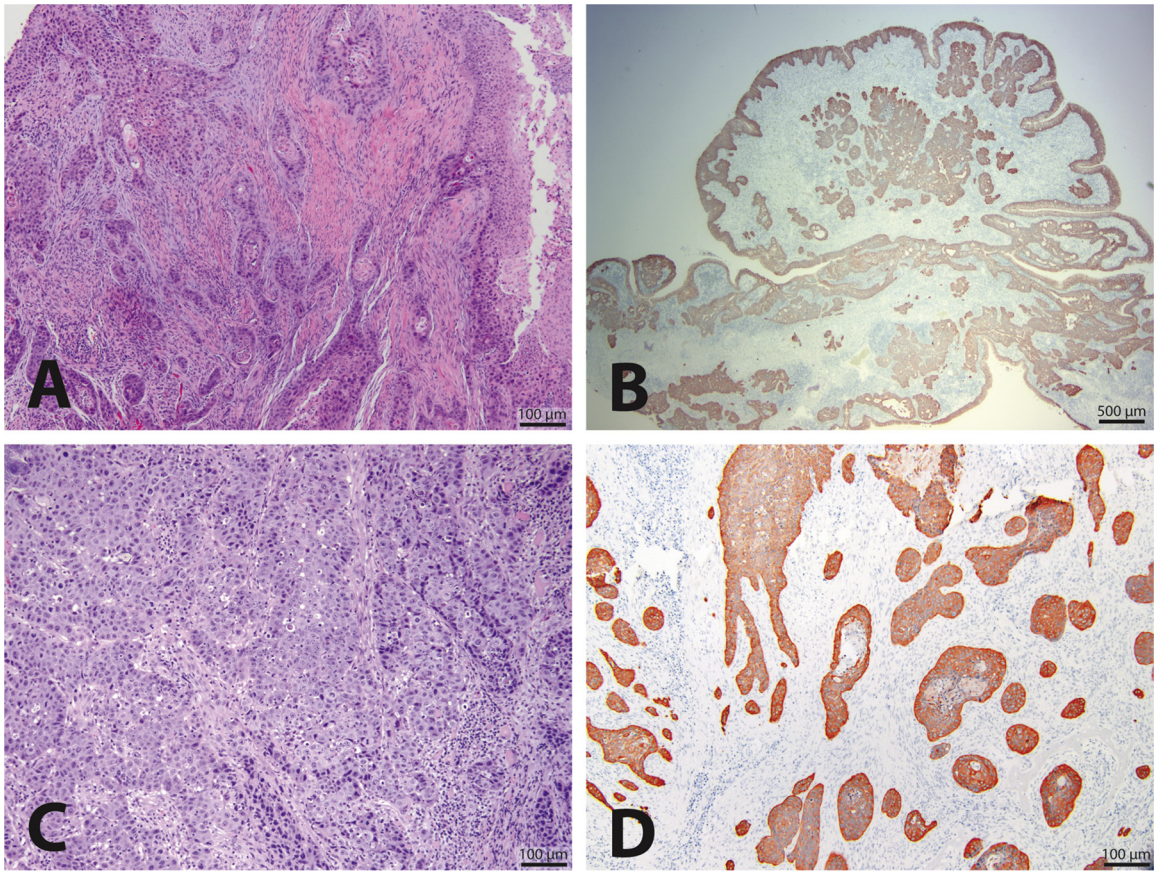

Fig. 1. Histologic subtypes of feline OSCC. A representative image of the histologic appearance of a well-differentiated conventional feline OSCC stained with H&E is shown (10× magnification) (A). A representative image for a papillary subtype of feline OSCC also stained for cytokeratins by IHC is shown (20× magnification) (B). A representative image for a basaloid subtype of feline OSCC stained with H&E is shown (100× magnification) (C). A representative image of a well-differentiated conventional feline OSCC shows all neoplastic epithelium staining positive for cytokeratins when stained with an anti-pan-cytokeratin antibody and analyzed by IHC (100× magnification) (D).

the forkhead transcription factor FoxP3, a protein considered to be required for the development and function of Tregs and as well as a key marker for this immunoregulatory CD4 T cell subset (Hori et al., 2003; Li and Zheng, 2015). The frequency of detection of FoxP3-expressing cells in this feline OSCC cohort was 58% (7/12) with scores ranging from 1+ (5/7 cases) to 2+ (2/7) (Table 3). FoxP3 expression was identified in the nucleus as expected and previously reported in feline cells (Lankford et al., 2008). Positive cells were generally individualized and scattered within the inflamed interstitium (tumor stroma), and in some cases also infiltrating within the neoplastic epithelium. Within the tumor stroma, FoxP3-expressing cells were typically intermixed within sheets of lymphocytes. However, FoxP3-expressing cells within the neoplastic epithelium were generally individualized and isolated from other inflammatory cells. A correlation was not detected between Treg infiltrates and other individual immune cell infiltrates with the exception of a positive association determined between FoxP3 and CD3 IHC scores ($r = 0.624$; $P = 0.035$). FoxP3 expression was not observed in the normal control tissues including tongue and oral mucosa. Multiple clusters of FoxP3-expressing cells were evident within the tumor stroma of case 6 as shown in Fig. 2E.

COX-2 expression was detected in a proportion of cases (9/12; 75%) within this feline OSCC cohort and scored based on expression within carcinoma epithelium, rather than tumor stroma (Table 3). COX-2 expression was generally weak with rare or infrequent tumor cells staining positive for this immunomodulator with most cases (8/9) scored as 1+ and only one case showing a 2+ score (Table 3). In addition, COX-2 expression was detected in tumor stroma in seven of the case biopsies (cases 1, 3–4, 7–8, 11–12) also shown to demonstrate tumor cell COX-2 expression. Notably, COX-2 expression was scored as "0" for two patients (cases 9–10) due to the absence of staining of tumor epithelium, although COX-2 positive cells were observed within the tumor stroma of these two case biopsies (Table 3). Staining patterns for both tumor epithelium and tumor stroma generally revealed scattered positive cells with cytoplasmic expression of variable intensity as shown for case 11 in Fig. 3F. Cells within tumor stroma that stained positive for COX-2 were typically fibroblasts based on morphology, although further characterization of fibroblasts as cancer associated fibroblasts (CAFs) by IHC analysis for α-smooth muscle actin (α-SMA) was not conducted. COX-2 IHC scores did not correlate with scores for any individual immune cell infiltrates.

3.4. Flow cytometric analysis of circulating Treg frequencies in OSCC

To further explore immunologic events associated with feline OSCC, circulating Treg frequencies were characterized by multicolor flow cytometry for both feline OSCC patients (cohort-2; n = 9) and healthy control cats including both adult SPF and non-SPF cats. Scatter plots representative of the gating strategy used for analysis of Treg subsets defined by CD25 and FoxP3 staining within the CD3+CD4+ population, are shown in Fig. 4A. This staining panel and gating strategy allowed analysis of frequencies of three different CD4 T cell subsets including total FoxP3+ (CD25+ and CD25- gates), CD25+FoxP3+, and CD25-FoxP3+ cell populations. Findings revealed comparable frequencies of CD25+FoxP3+ cells within the CD4 T cell subset between feline OSCC patients (median = 4.14%) and control groups including all controls (median = 3.97%), adult SPF cats only (median = 4.03%)

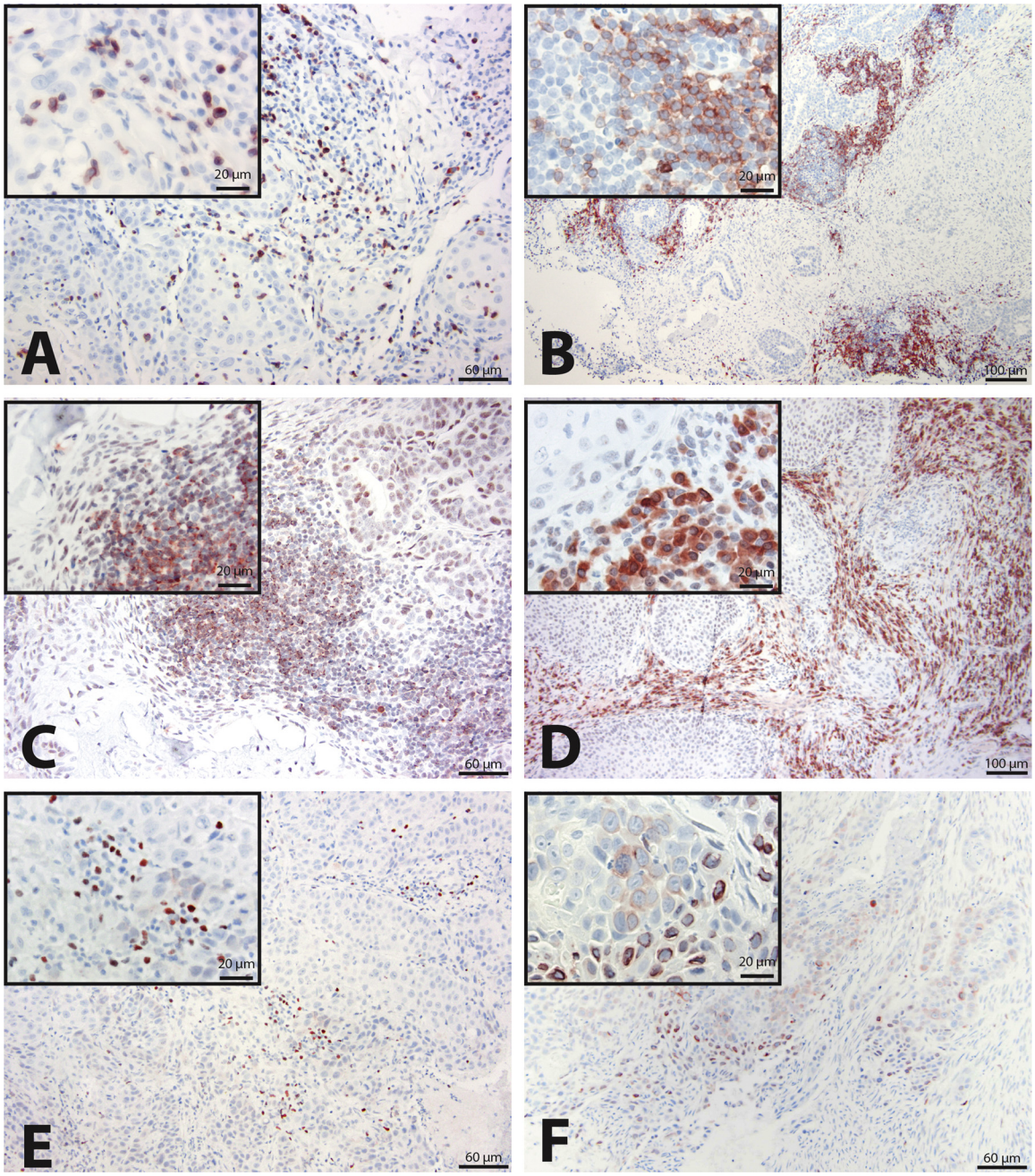

Fig. 2. Lymphoid cell infiltration and COX-2 expression in feline OSCC by IHC analysis. A representative image of a feline OSCC shows T cell infiltration within neoplastic epithelium and stroma by staining with a feline cross-reactive CD3 monoclonal antibody and IHC analysis (200× magnification) (A). A representative image of T cell infiltration restricted predominantly to neoplastic stroma is shown (100× magnification) by CD3 IHC analysis (B). B cell follicle-like structure within neoplastic stroma is depicted by staining with a feline cross-reactive CD79a monoclonal antibody and IHC analysis (200× magnification) (C). Large numbers of B cells infiltrate neoplastic stroma in the absence of follicle-like structures as shown by CD79a IHC analysis (100× magnification) (D). Scattered Fox-P3+ cells infiltrate neoplastic stroma as shown by staining with a feline cross-reactive Fox-P3 monoclonal antibody and IHC analysis (200× magnification) (E). A representative image of variable COX-2 expression in neoplastic epithelium is shown by staining with a feline cross-reactive COX-2 monoclonal antibody and IHC analysis (200X magnification) (F). Insets within each image are a 400× magnification of a selected site within the parental image.

and adult non-SPF only (median = 3.29%) (Fig. 4B). However, frequency of the total FoxP3+ CD4 subset for OSCC patients (median = 8.71%) was significantly greater ($P = 0.045$) when compared to the frequency observed for the adult non-SPF control group (median = 5.16%) (Fig. 4C). Similarly, the frequency of the CD4+CD25-FoxP3 subset (median = 3.85%) determined for OSCC patients was significantly greater ($P = 0.004$) when compared to the frequency observed for the adult non-SPF control group (median = 1.97%) (Fig. 4D). Significant differences were not observed when median frequencies calculated for either the total FoxP3+ CD4 or for the CD4+CD25-FoxP3+ T cell subsets for the OSCC patient cohort were compared to frequencies derived for the group inclusive of all controls or for the SPF adult controls (Fig. 4C-D). Interestingly, a significant difference ($P = 0.006$) was observed between the CD4+CD25-FoxP3+ subset frequencies calculated for the adult SPF (median = 6.34%) and non-SPF controls (median = 2.44%) (Fig. 4D), a finding that characterized circulating FoxP3+CD4 + T cells as predominantly negative for CD25 expression in this small adult SPF cohort.

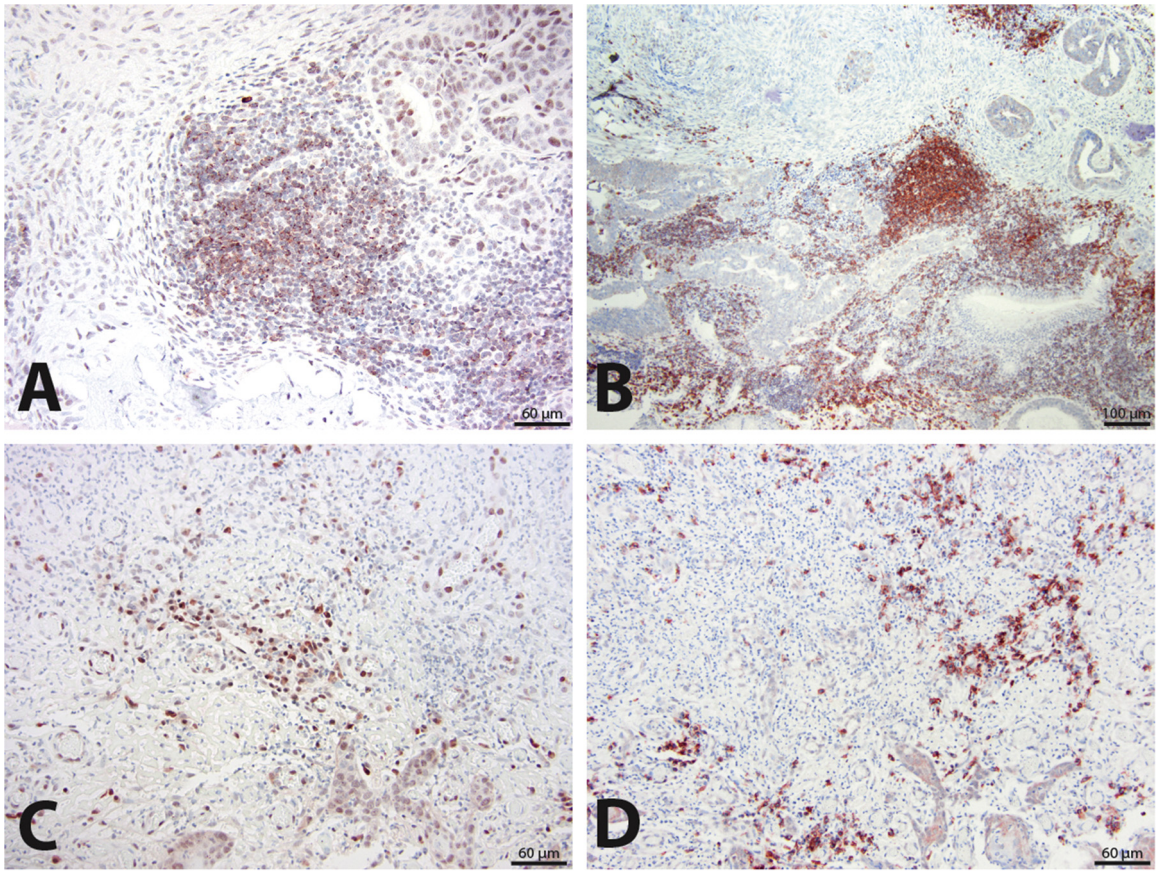

Fig. 3. Comparison of staining with CD79a and CD20 antibodies for characterization of B cell infiltrates. Tissue sections from the same feline OSCC patient biopsy analyzed by CD79a IHC (200× magnification) (A) and CD20 IHC (100× magnification) (B) are compared for detection of B cell infiltrates that also reveal follicle-like structures within neoplastic stroma. Similarly, tissue sections from a second patient biopsy analyzed with CD79a IHC (200× magnification) (C) and CD20 IHC (200× magnification) (D) are compared for detection of B cell infiltrates characterized by scattered B cells within neoplastic stroma.

4. Discussion

Multiple reports have shown T cell and Treg infiltrates to confer prognostic significance in human HNSCC and other cancers (Ferris, 2015; Shang et al., 2015; Wallis et al., 2015). Tumor-infiltrating lymphocytes, in particular CD8 T cells, generally correlate with a favorable prognosis in human HNSCC, although this finding may depend on the localization and stage of the cancer (Wallis et al., 2015; Lei et al., 2016; De Meulenaere et al., 2017). Examination of lymphocytic infiltrates within feline OSCC samples has not been reported previously. The overall hypothesis behind these studies was that feline OSCC and human HNSCC share similar immune profiles based on lymphocyte subset infiltration. Therefore, a preliminary investigation that specifically examined the frequency, intensity, and localization of T cell, Treg and B cell infiltrates within feline OSCC patient cohort served as critical aim to test this hypothesis.

T cell infiltration based on detection CD3+ cells by IHC analysis, was detected for all patient biopsies except one, although the frequency of T cells within each patient sample was variable with scores ranging from 1+ to 3 + . Two patterns of T cell infiltration were identified for this feline cohort-1 with one pattern characterized by infiltration of both tumor stroma and neoplastic epithelium and a second pattern showing infiltration predominately within the tumor stroma. Reports describing T cell infiltration of specific tumor compartments for human HNSCC are limited but also revealed differences in distribution of T cells within tumor compartments including tumor stroma, tumor epithelium and tumor margins. However, reports for human HNSCC also revealed conflicting results regarding correlation of disease progression and localization of T cell infiltration to specific compartments (Lei et al., 2016; De Meulenaere et al., 2017). Therefore, the importance of specific tumor compartments for T cell localization in human and feline OSCC remains undetermined. Importantly, our study confirmed T cell infiltration as a common finding for feline OSCC, although the significance of the variability observed for infiltrating T cell numbers between cases will require further investigation.

Tumor-infiltrating Tregs defined by expression of transcription factor FoxP3, comprise a critical CD4 T cell subset that is both immunosuppressive and anti-inflammatory. Tregs contribute to the immunosuppressive microenvironment of multiple cancers by various mechanisms including production of IL-10 and TGF-β, deprivation of effector T cells for T cell growth factors such as IL-2, and expression of immunosuppressive molecules including CTLA-4, PD-1, CD39 and surface bound TGF-β (Rodriguez-Perea et al., 2016). Although FoxP3 is considered a key marker for identification of Tregs, it should be noted that this transcription factor may also be transiently expressed on activated conventional CD4 T cells (Rodriguez-Perea et al., 2016). Regardless, Treg frequency often correlates with an unfavorable prognosis in multiple types of cancers including human HNSCC (Allen et al., 2015; Davis et al., 2016). However, conflicting reports have shown that FoxP3+ cell infiltration may actually be associated with improved prognosis in some case cohorts of human HNSCC, possibly due to modulation of tumor-promoting inflammatory responses (Shang et al., 2015; Davis et al., 2016; De Meulenaere et al., 2017). Intensity of Treg infiltration of human HNSCC was also reported to correlate with tumor grade, tumor associated inflammation and tumor localization (Al-Qahtani et al., 2011; Wallis et al., 2015; De Meulenaere et al., 2017). Regarding our feline cohort-1, only a subset of OSCC patient samples (7/12) revealed intratumoral infiltration of FoxP3+ cells with scores

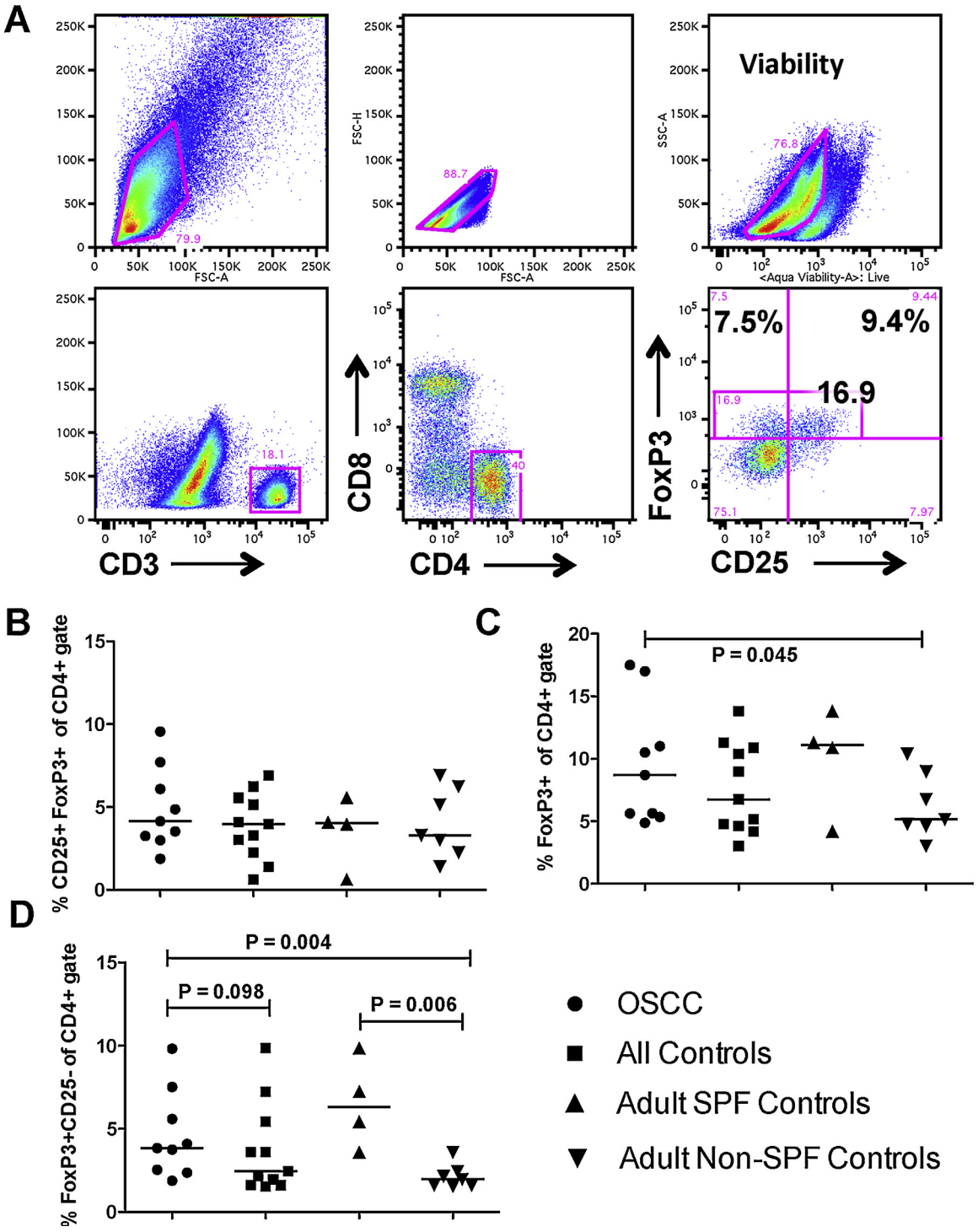

Fig. 4. Frequencies of circulating FoxP3+ CD4 T cells in feline OSCC patients. A representative scatter plot of a patient's PBMC shows the gating protocol for interrogation of PBMC for CD3+CD4 + T cells for FoxP3 and CD25 expression using multi-color flow cytometry as described in Materials and Methods (A). Median frequencies of CD25+FoxP3+ cells within the CD4 T cell subset are compared between the feline OSCC patient cohort-2 and either all control cats, adult SPF controls, or adult non-SPF controls (healthy pet cats) (B). Similarly, median frequencies of FoxP3+ cells (both CD25+ and CD25- populations) within the CD4 T cell subset are compared between cohort-2 patients and different control groups (C). Median frequencies of the FoxP3+CD25- population with the CD4 T cell subset are compared between cohort-2 patients and different control groups (D). Pair-wise analysis between different groups was conducted with the Mann Whitney test using Graph Pad Prism software and one-tailed analysis. *P* values < 0.05 are considered significant.

ranging from 1+ to 2 + . FoxP3+ cells were presumed to be CD4 T cells and were generally associated with other infiltrating lymphocytes when detected within tumor stroma. Furthermore, the positive correlation between CD3 and FoxP3 IHC scores would suggest that a proportion of stromal T cells are CD4 T cells. However, the isolation of FoxP3+ cells from other inflammatory cells when localized to tumor epithelium is not readily explained. Future studies focused on localization of T cell infiltrates and tumor compartment-specific distribution of particular T cell subsets including CD4 and CD8 T cells and Tregs, will be required to characterize T cell infiltration as a factor for biologic

behavior of feline OSCC.

Notably, intratumoral B cell infiltrates were observed in all examined OSCC cases in this study based on CD79a and CD20 expression determined by IHC. Infiltrating B cells have been reported for human HNSCC, but less frequently and in lower numbers compared to infiltrating T cells. One report (Quan et al., 2016) as well as a second report (Kroeger et al., 2016), found that B cells were usually distributed in aggregates or sparsely throughout tumors, although some samples exhibited lymphoid follicle-like structures consisting of CD20+ B-cells. Our study also included two cases demonstrating B cells aggregated into follicle-like structures. In addition, feline OSCC cases within cohort-1 demonstrated B cell infiltration restricted to tumor stroma only, in contrast to T cell infiltrates that were frequently detected within tumor epithelium and stroma. This finding is noteworthy given that feline chronic gingivostomatitis (FCGS), a chronic severe oral mucosal inflammatory disease in cats, is associated with plasma cell infiltrates that are also typically localized to subepithelial stroma and not epithelium. In contrast, T cell infiltrates observed for FCGS biopsies were shown to be localized to epithelium and subepithelial stroma (Harley et al., 2011; Arzi et al., 2017), similar to our findings for feline OSCC. Reasons for variability in B cell infiltration between different feline OSCC patients with scores ranging from 1+ to 3+ are unknown. However, host factors such as concurrent inflammatory conditions and differences of the oral microbiome defined by variation of commensal bacterial populations and chronic viral infections, may modulate the nature of infiltrating immune cells. Furthermore, the significant association observed between CD3 and CD79a IHC scores suggests that B cell infiltration may play an important role in the host adaptive response including T cell responses, to either tumor or microbial antigens associated with feline OSCC.

Additionally, analysis of cohort-1 samples revealed similar scores for staining with CD79a and CD20. These results suggested that these infiltrates were predominantly B cells rather than plasma cells given that B cells typically lose CD20 expression upon differentiation into plasma cells (Jourdan et al., 2011). Nevertheless, additional examination of feline OSCC samples by IHC with markers specific for plasma cells is warranted to fully determine the involvement of this cell type in feline OSCC. The role of infiltrating B cells in feline OSCC development and progression is worthy of future investigation based on recent reports showing B cell and plasma cell infiltration as prognostic markers in various human cancers (Shalapour et al., 2015; Schwartz et al., 2016).

In contrast to COX-1 that is expressed constitutively in most normal tissues, COX-2 is only expressed in response to inflammatory and mitogenic stimulation. COX-2 catalyzes the synthesis of prostaglandins including PGE-2, which is a proinflammatory prostaglandin that is frequently associated with field cancerization. PGE-2 induces extended cell survival, cell proliferation and migration and neo-angiogenesis through multiple mechanisms (Feller et al., 2013). COX-2 expression has been shown to correlate with tumor stage, lymph node metastasis, local reoccurrence and survival in human HNSCC, although reports conflict regarding a direct correlation of tumor associated COX-2 expression and patient survival (Feller et al., 2013; Yang et al., 2016). Furthermore, tumor-associated COX-2 expression and resulting PGE-2 secretion may involve neoplastic keratinocytes, tumor-associated fibroblasts and infiltrating inflammatory cells resulting in critical interactions between tumor epithelium and tumor microenvironment to promote tumor progression as described for human HNSCC (Alcolea et al., 2012; Leef and Thomas, 2013). COX-2 expression may also promote tumor progression through activation of FoxP3 expression and induction of tumor-associated Tregs in various cancers including human HNSCC (Baratelli et al., 2005; Feller et al., 2013). Previous reports have described COX-2 expression in feline OSCC, although the frequency of detection of COX-2 expression was variable between different studies with frequencies ranging from 9 to 82% of cases examined (Beam et al., 2003; Hayes et al., 2006; DiBernardi et al., 2007; Millanta et al., 2016). Our findings revealed weak COX-2 expression for 75% of cases tested with only one case (8%) showing higher expression (score of 2) for COX-2. Similarly, a previous study reported higher COX-2 expression for only 18% of feline OSCC cases examined (DiBernardi et al., 2007). Importantly, our studies revealed COX-2 expression in both tumor epithelium and stroma with positive stroma cells identified as fibroblasts based on morphology. COX-2 expression within the stroma of feline OSCC has not been previously described, although a more recent study described COX-2 expression in all feline OSCC cell lines including a cell line derived from tumor associated fibroblasts (Martin et al., 2015). Examination of larger patient cohorts and further investigation of cell types expressing COX-2 will be necessary to determine the role of this immune mediator as a prognostic factor and therapeutic target for feline OSCC.

Increased frequencies of circulating Treg have been reported in human HNSCC although the correlation of Treg frequencies in blood and disease progression remains unclear (Strauss et al., 2007; Drennan et al., 2013). Our investigation also revealed increased frequencies of circulating Tregs in a proportion of patients within the feline OSCC cohort-2. Tregs have been identified by flow cytometric analysis using different criteria including a classical definition as CD4 + CD25^{hi} T cells, CD4 + CD25 + CD127^{lo} T cells, CD4 + CD25 + FoxP3 + T cells, or characterized by FoxP3 expression alone and defined as CD4 + FoxP3 + T cells (Rodriguez-Perea et al., 2016). Using the definition of CD4 + CD25 + FoxP3 + T cells, median frequencies of Tregs were not significantly different between patients and SPF and non-SPF control cats. However, frequencies of the CD4 + FoxP3 + T cell population inclusive of CD25+ and CD25- CD4 T cell populations (total FoxP3 + CD4 T cells), and the CD4 + CD25-FoxP3 + T cell population were found to be higher for feline OSCC patients compared to controls, particularly compared to controls consisting of non-SPF pet cats. These results pointed to the detection of a CD4 + CD25-FoxP3 + T cell subset that is not aligned with the classical definition of Tregs but has been described in the literature with several possible identities. These identities include a recently activated population of CD4 T cells that is not yet fully committed to becoming Tregs (Li and Zheng, 2015) or an IL-10 producing CD4 T cell subset regulated by transcription factor Egr-2 and capable of inducing anergy as described for other classical Tregs (Okamura et al., 2009, 2015). Tregs negative for CD25 expression have also been described as a reservoir of committed regulatory cells that will gain CD25 expression upon activation (Zelenay et al., 2005). Differences between CD25+ and CD25- feline Tregs are currently unknown, although we have detected a similar circulating CD25-FoxP3 + CD4 T cell population in pet dogs (E. Sparger, unpublished results). Furthermore, comparison of our findings for feline Treg frequencies with other reports describing this subset in cats is problematic as most published studies define this population as CD4 + CD25+ or CD4 + CD25^{hi} T cells when using flow cytometric analysis (Mexas et al., 2008; Fogle et al., 2010a, b; Miller et al., 2013, 2014). Nevertheless, our findings show alterations in the circulating FoxP3 + CD4 T cell subset in feline OSCC patients and provide justification for future studies of this immune cell subset as a peripheral marker for this feline cancer. An unexpected outcome was the higher frequencies of the total FoxP3 + CD4 T cell subset observed in the SPF control cohort when compared to the non-SPF pet cat controls. This finding is not easily explained although a recent report comparing SPF rhesus macaques to age-matched conventionally raised macaques within the same primate center, revealed differences for T cell maturation and functions between the two macaque populations (Oxford et al., 2015). Testing of a larger cohort of older SPF cats will be necessary to confirm this finding, which may have implications regarding the use of SPF cats for characterizing normal values for feline immune cell subsets.

There are several key limitations to the phenotypic analysis of circulating T cells in this study. Firstly, the determination of circulating CD8 T cell frequencies was not possible due to results showing inconsistent staining of CD8 T cells during phenotypic analysis of blood by

flow cytometry. Secondly, the absence of contemporaneous complete blood cell counts precluded the calculation of absolute counts of Tregs in the blood. However, the primary goal of this current study was the determination of circulating Treg frequencies defined by FoxP3+ CD4 T cells, which is a Treg measurement most frequently reported and utilized to characterize this immunosuppressive population in cancer and other disease states. Future analysis of the ratio of frequencies of circulating CD8 T cell and Tregs will be warranted to characterize the balance between these effector and regulatory populations and to evaluate the immune competence of feline OSCC patients. Moreover, simultaneous evaluation of circulating and intratumoral immune cell populations should be conducted to generate a more comprehensive immune profile associated with this cancer.

Classification of feline OSCC according to subtype has not been previously reported. Therefore, a separate aim of this investigation was the characterization of feline OSCC cases according to subtype as previously described for canine oral non-tonsillar squamous cell carcinoma (Barnes et al., 2005; Nemec et al., 2012). Findings from the feline OSCC cohort-1 revealed a distribution characterized by predominately conventional subtypes (75%) split evenly between well-differentiated and moderately differentiated carcinomas. In contrast, only two cases were classified as papillary and one case as basaloid subtypes. These results were very similar to those reported for a much larger cohort (n = 84) of canine OSCC cases, which also revealed a predominance of canine cases to be conventional (82.1%) equally distributed between well and moderately differentiated carcinomas, and a much smaller proportion of cases to be either papillary or basaloid (5.95% each). However, this canine cohort contained two additional subtypes including adenosquamous (3.6%) and spindle cell (2.4%) carcinomas that were missing from our study, possibly due to the size of this feline OSCC cohort. Reports relating to subtype correlation with biologic behavior of human head and neck SCC are few but indicate that the conventional and basaloid subtypes are associated with high metastatic potential and poor prognosis, whereas the papillary subtype variant is associated with a more favorable prognosis (Pereira et al., 2007; Fitzpatrick et al., 2013). However, papillary subtypes are far less common in human, canine and feline OSCC. Examination of a larger cohort of clinical cases of feline OSCC for subtype will be needed to accurately determine the incidence of subtype variants of very low frequency in dogs and humans such as adenosquamous and spindle cell.

A correlation between subtype, IHC immune marker scores or circulating Treg frequencies with clinical characteristics or outcome was not observed. However, this finding was not surprising based on the limited number of cases within cohorts-1 and 2. Previous reports have described localization of tumor to the tongue as a correlate for either overall survival or angiogenesis for feline OSCC (Bergkvist et al., 2011; Yoshikawa et al., 2012; Klobukowska and Munday, 2016) and included larger case cohorts with higher numbers of cases characterized by lingual tumors. Future studies are needed to evaluate possible correlations between immune markers and prognosis in cats with OSCC. The small number of cases, variability of treatments and lack of uniform clinical follow-up did not allow useful comparisons between prognosis and immune marker findings for the cohorts evaluated in this study. Similarly, few investigations of feline OSCC so far have identified correlates of clinical outcome, most likely due to size of cohorts examined and due to poor responses elicited by treatments tested so far. Accordingly, future studies testing larger case cohorts that are also diverse in tumor localization, tumor stage, clinical course, and survival time will be needed to determine immune correlates of clinical outcome for this feline cancer.

5. Conclusion

Recent successes with immunotherapeutics targeting immunoregulatory elements of cancer, specifically antibodies blocking activity of T-cell immunosuppressive markers CTLA-4, PD-1 and PD-L1, confirm the role of the host immune response in the control of cancer (Farkona et al., 2016; Tsai and Hsu, 2017). Feline OSCC biopsies revealed infiltration of multiple lymphoid subsets including T and B cells as well as FoxP3+ cells that likely represent a Treg subset. Expression of COX-2, another important immune modulator, is also detected in a proportion of feline OSCC patient biopsies although expression was typically weak. Finally, examination of patient biopsies for histologic subtypes demonstrated the conventional squamous cell carcinoma as the most frequent subtype similar to findings for canine OSCC and human HNSCC. Examination of additional immune markers including CD8 T cells, natural killer cells, macrophage and monocytic subsets including myeloid-derived suppressor cells, dendritic cells and activation (including PD-1 and PD-L1) phenotypes of various immune cells, will be required to more fully define immune profiles of feline OSCC patients. Furthermore, examination of larger and more diverse feline OSCC patient cohorts will be necessary to characterize immune correlates of disease outcomes. Nevertheless, findings from this current study provide a preliminary step to these goals and demonstrate for the first time, similarities in immune markers shared by feline OSCC and human HNSCC. Lastly, these results relating to cancer-associated immune markers provide further support for spontaneous feline OSCC as a model for human HNSCC for investigation of innovative immunotherapeutics that may benefit both human and feline patients.

Conflicts of interest

The authors declare no conflict of interest.

Acknowledgements

The authors acknowledge the technical assistance of Teri Guerrero (Clinical Trials Support; VMTH; UC Davis) and Debbie Bee (UC Davis Feline Nutrition and Pet Care Center). This study was funded by the Center for Companion Animal Health (CCAH), School of Veterinary Medicine, UC Davis and the National Institutes of Health (Clinical Translational Science Award; UL1 RR024146 and UL1 TR001860). The authors are also grateful for the cat owners that permitted blood collection from their pet cats. Funding sources for experimental work described in this paper had no role in experimental design, collection of data, analysis and interpretation of data, writing of the manuscript or selection of journal for submission.

References

Alcolea, S., Anton, R., Camacho, M., Soler, M., Alfranca, A., Aviles-Jurado, F.X., Redondo, J.M., Quer, M., Leon, X., Vila, L., 2012. Interaction between head and neck squamous cell carcinoma cells and fibroblasts in the biosynthesis of PGE2. J. Lipid Res. 53, 630–642.

Allen, C.T., Clavijo, P.E., Van Waes, C., Chen, Z., 2015. Anti-tumor immunity in head and neck cancer: understanding the evidence, how tumors escape and immunotherapeutic approaches. Cancers (Basel) 7, 2397–2414.

Al-Qahtani, D., Anil, S., Rajendran, R., 2011. Tumour infiltrating CD25+ FoxP3+ regulatory T cells (Tregs) relate to tumour grade and stromal inflammation in oral squamous cell carcinoma. J. Oral. Pathol. Med. 40, 636–642.

Altamura, G., Corteggio, A., Pacini, L., Conte, A., Pierantoni, G.M., Tommasino, M., Accardi, R., Borzacchiello, G., 2016. Transforming properties of Felis catus papillomavirus type 2 E6 and E7 putative oncogenes in vitro and their transcriptional activity in feline squamous cell carcinoma in vivo. Virology 496, 1–8.

Arzi, B., Murphy, B., Baumgarth, N., Vapniarsky, N., Nemec, A., Naydan, D.K., Cox, D.P., Verstraete, F.J., 2011. Analysis of immune cells within the healthy oral mucosa of specific pathogen-free cats. Anat. Histol. Embryol. 40, 1–10.

Arzi, B., Clark, K.C., Sundaram, A., Spriet, M., Verstraete, F.J.M., Walker, N.J., Loscar, M.R., Fazel, N., Murphy, W.J., Vapniarsky, N., Borjesson, D.L., 2017. Therapeutic efficacy of fresh, allogeneic mesenchymal stem cells for severe refractory feline chronic gingivostomatitis. Stem Cells Transl. Med. 6, 1710–1722.

Baratelli, F., Lin, Y., Zhu, L., Yang, S.C., Heuze-Vourc'h, N., Zeng, G., Reckamp, K., Dohadwala, M., Sharma, S., Dubinett, S.M., 2005. Prostaglandin E2 induces FOXP3 gene expression and T regulatory cell function in human CD4+ + T cells. J. Immunol. 175, 1483–1490.

Bardagi, M., Fondevila, D., Ferrer, L., 2012. Immunohistochemical detection of COX-2 in feline and canine actinic keratoses and cutaneous squamous cell carcinoma. J. Comp. Pathol. 146, 11–17.

Barnes, L., Eveson, J.W., Reichart, P., Sidransky, D., 2005. World Health Organization Classification of Tumours. Pathology and Genetics of Head and Neck Tumours. IARC

Press, Lyon, France.
Beam, S.L., Rassnick, K.M., Moore, A.S., McDonough, S.P., 2003. An immunohistochemical study of cyclooxygenase-2 expression in various feline neoplasms. Vet. Pathol. 40, 496–500.
Bergkvist, G.T., Argyle, D.J., Morrison, L., MacIntyre, N., Hayes, A., Yool, D.A., 2011. Expression of epidermal growth factor receptor (EGFR) and Ki67 in feline oral squamous cell carcinomas (FOSCC). Vet. Comp. Oncol. 9, 106–117.
Bilgic, O., Duda, L., Sanchez, M.D., Lewis, J.R., 2015. Feline oral squamous cell carcinoma: clinical manifestations and literature review. J. Vet. Dent. 32, 30–40.
Cooper, J.S., Porter, K., Mallin, K., Hoffman, H.T., Weber, R.S., Ang, K.K., Gay, E.G., Langer, C.J., 2009. National cancer database report on cancer of the head and neck: 10-year update. Head Neck 31, 748–758.
Davis, R.J., Van Waes, C., Allen, C.T., 2016. Overcoming barriers to effective immunotherapy: MDSCs, TAMs, and Tregs as mediators of the immunosuppressive microenvironment in head and neck cancer. Oral Oncol. 58, 59–70.
De Meulenaere, A., Vermassen, T., Aspeslagh, S., Vandecasteele, K., Rottey, S., Ferdinande, L., 2017. TILs in head and neck cancer: ready for clinical implementation and why (not)? Head Neck Pathol. 11, 354–363.
DiBernardi, L., Doré, M., Davis, J.A., Owens, J.G., Mohammed, S.I., Guptill, C.F., Knapp, D.W., 2007. Study of feline oral squamous cell carcinoma: potential target for cyclooxygenase inhibitor treatment. Prostaglandins Leukot. Essent. Fatty Acids 76, 245–250.
Drennan, S., Stafford, N.D., Greenman, J., Green, V.L., 2013. Increased frequency and suppressive activity of CD127(low/-) regulatory T cells in the peripheral circulation of patients with head and neck squamous cell carcinoma are associated with advanced stage and nodal involvement. Immunology 140, 335–343.
Farkona, S., Diamandis, E.P., Blasutig, I.M., 2016. Cancer immunotherapy: the beginning of the end of cancer? BMC Med. 14, 73.
Feller, L., Altini, M., Lemmer, J., 2013. Inflammation in the context of oral cancer. Oral Oncol. 49, 887–892.
Ferris, R.L., 2015. Immunology and immunotherapy of head and neck cancer. J. Clin. Oncol. 33, 3293–3304.
Fitzpatrick, S.G., Neuman, A.N., Cohen, D.M., Bhattacharyya, I., 2013. Papillary variant of squamous cell carcinoma arising on the gingiva: 61 cases reported from within a larger series of gingival squamous cell carcinoma. Head Neck Pathol. 7, 320–326.
Fogle, J.E., Mexas, A.M., Tompkins, W.A., Tompkins, M.B., 2010a. CD4(+)CD25(+) T regulatory cells inhibit CD8(+) IFN-gamma production during acute and chronic FIV infection utilizing a membrane TGF-beta-dependent mechanism. AIDS Res. Hum. Retroviruses 26, 201–216.
Fogle, J.E., Tompkins, W.A., Tompkins, M.B., 2010b. CD4+CD25+ T regulatory cells from FIV++ cats induce a unique anergic profile in CD8+ lymphocyte targets. Retrovirology 7, 97.
Gould, S.E., Junttila, M.R., de Sauvage, F.J., 2015. Translational value of mouse models in oncology drug development. Nat. Med. 21, 431–439.
Harley, R., Gruffydd-Jones, T.J., Day, M.J., 2011. Immunohistochemical characterization of oral mucosal lesions in cats with chronic gingivostomatitis. J. Comp. Pathol. 144, 239–250.
Hayes, A.M., Scase, T.J., Miller, J., Murphy, S., Sparkes, A., Adams, V., 2006. COX-1 and COX-2 expression in feline oral squamous cell carcinoma. J. Comp. Pathol. 135, 93–99.
Hori, S., Nomura, T., Sakaguchi, S., 2003. Control of regulatory T cell development by the transcription factor Foxp3. Science 299, 1057–1061.
Jourdan, M., Caraux, A., Caron, G., Robert, N., Fiol, G., Reme, T., Bollore, K., Vendrell, J.P., Le Gallou, S., Mourcin, F., De Vos, J., Kassambara, A., Duperray, C., Hose, D., Fest, T., Tarte, K., Klein, B., 2011. Characterization of a transitional preplasmablast population in the process of human B cell to plasma cell differentiation. J. Immunol. 187, 3931–3941.
Khanna, C., Lindblad-Toh, K., Vail, D., London, C., Bergman, P., Barber, L., Breen, M., Kitchell, B., McNeil, E., Modiano, J.F., Niemi, S., Comstock, K.E., Ostrander, E., Westmoreland, S., Withrow, S., 2006. The dog as a cancer model. Nat. Biotechnol. 24, 1065–1066.
Klobukowska, H.J., Munday, J.S., 2016. High numbers of stromal cancer-associated fibroblasts are associated with a shorter survival time in cats with oral squamous cell carcinoma. Vet. Pathol. 53, 1124–1130.
Kroeger, D.R., Milne, K., Nelson, B.H., 2016. Tumor-infiltrating plasma cells are associated with tertiary lymphoid structures, cytolytic t-cell responses, and superior prognosis in ovarian cancer. Clin. Cancer Res. 22, 3005–3015.
Lankford, S., Petty, C., LaVoy, A., Reckling, S., Tompkins, W., Dean, G.A., 2008. Cloning of feline FOXP3 and detection of expression in CD4+CD25+ regulatory T cells. Vet. Immunol. Immunopathol. 122, 159–166.
LeBlanc, A.K., Breen, M., Choyke, P., Dewhirst, M., Fan, T.M., Gustafson, D.L., Helman, L.J., Kastan, M.B., Knapp, D.W., Levin, W.J., London, C., Mason, N., Mazcko, C., Olson, P.N., Page, R., Teicher, B.A., Thamm, D.H., Trent, J.M., Vail, D.M., Khanna, C., 2016. Perspectives from man's best friend: national academy of medicine's workshop on comparative oncology. Sci. Transl. Med. 8 324ps.
Lechner, A., Schlosser, H., Rothschild, S.I., Thelen, M., Reuter, S., Zentis, P., Shimabukuro-Vornhagen, A., Theurich, S., Wennhold, K., Garcia-Marquez, M., Tharun, L., Quaas, A., Schauss, A., Isensee, J., Hucho, T., Huebbers, C., von Bergwelt-Baildon, M., Beutner, D., 2017. Characterization of tumor-associated T-lymphocyte subsets and immune checkpoint molecules in head and neck squamous cell carcinoma. Oncotarget 8, 44418–44433.
Leef, G., Thomas, S.M., 2013. Molecular communication between tumor-associated fibroblasts and head and neck squamous cell carcinoma. Oral Oncol. 49, 381–386.
Lei, Y., Xie, Y., Tan, Y.S., Prince, M.E., Moyer, J.S., Nor, J., Wolf, G.T., 2016. Telltale tumor infiltrating lymphocytes (TIL) in oral, head & neck cancer. Oral Oncol. 61, 159–165.
Li, X., Zheng, Y., 2015. Regulatory T cell identity: formation and maintenance. Trends Immunol. 36, 344–353.
Martin, C.K., Dirksen, W.P., Carlton, M.M., Lanigan, L.G., Pillai, S.P., Werbeck, J.L., Simmons, J.K., Hildreth, B.E., London 3rd, C.A., Toribio, R.E., Rosol, T.J., 2015. Combined zoledronic acid and meloxicam reduced bone loss and tumour growth in an orthotopic mouse model of bone-invasive oral squamous cell carcinoma. Vet. Comp. Oncol. 13, 203–217.
Mexas, A.M., Fogle, J.E., Tompkins, W.A., Tompkins, M.B., 2008. CD4+CD25+ regulatory T cells are infected and activated during acute FIV infection. Vet. Immunol. Immunopathol. 126, 263–272.
Millanta, F., Andreani, G., Rocchigiani, G., Lorenzi, D., Poli, A., 2016. Correlation between cyclo-oxygenase-2 and vascular endothelial growth factor expression in canine and feline squamous cell carcinomas. J. Comp. Pathol. 154, 297–303.
Miller, M.M., Fogle, J.E., Tompkins, M.B., 2013. Infection with feline immunodeficiency virus directly activates CD4+ CD25+ T regulatory cells. J. Virol. 87, 9373–9378.
Miller, M.M., Petty, C.S., Tompkins, M.B., Fogle, J.E., 2014. CD4+CD25+ T regulatory cells activated during feline immunodeficiency virus infection convert T helper cells into functional suppressors through a membrane-bound TGFbeta / GARP-mediated mechanism. Virol. J. 11, 7.
Moore, P.F., Woo, J.C., Vernau, W., Kosten, S., Graham, P.S., 2005. Characterization of feline T cell receptor gamma (TCRG) variable region genes for the molecular diagnosis of feline intestinal T cell lymphoma. Vet. Immunol. Immunopathol. 106, 167–178.
Moore, P.F., Rodriguez-Bertos, A., Kass, P.H., 2012. Feline gastrointestinal lymphoma: mucosal architecture, immunophenotype, and molecular clonality. Vet. Pathol. 49, 658–668.
Munday, J.S., French, A.F., 2015. Felis catus papillomavirus types 1 and 4 are rarely present in neoplastic and inflammatory oral lesions of cats. Res. Vet. Sci. 100, 220–222.
Nemec, A., Murphy, B., Kass, P.H., Verstraete, F.J., 2012. Histological subtypes of oral non-tonsillar squamous cell carcinoma in dogs. J. Comp. Pathol. 147, 111–120.
Okamura, T., Fujio, K., Shibuya, M., Sumitomo, S., Shoda, H., Sakaguchi, S., Yamamoto, K., 2009. CD4+CD25-LAG3+ regulatory T cells controlled by the transcription factor Egr-2. Proc. Natl. Acad. Sci. U. S. A. 106, 13974–13979.
Okamura, T., Sumitomo, S., Morita, K., Iwasaki, Y., Inoue, M., Nakachi, S., Komai, T., Shoda, H., Miyazaki, J., Fujio, K., Yamamoto, K., 2015. TGF-beta3-expressing CD4+CD25(-) LAG3+ regulatory T cells control humoral immune responses. Nat. Commun. 6, 6329.
Oxford, K.L., Dela Pena-Ponce, M.G., Jensen, K., Eberhardt, M.K., Spinner, A., Van Rompay, K.K., Rigdon, J., Mollan, K.R., Krishnan, V.V., Hudgens, M.G., Barry, P.A., De Paris, K., 2015. The interplay between immune maturation, age, chronic viral infection and environment. Immun. Ageing 12, 3.
Paoloni, M., Khanna, C., 2008. Translation of new cancer treatments from pet dogs to humans. Nat. Rev. Cancer 8, 147–156.
Pereira, M.C., Oliveira, D.T., Landman, G., Kowalski, L.P., 2007. Histologic subtypes of oral squamous cell carcinoma: prognostic relevance. J. Can. Dent. Assoc. 73, 339–344.
Quan, H., Fang, L., Pan, H., Deng, Z., Gao, S., Liu, O., Wang, Y., Hu, Y., Fang, X., Yao, Z., Guo, F., Lu, R., Xia, K., Tang, Z., 2016. An adaptive immune response driven by mature, antigen-experienced T and B cells within the microenvironment of oral squamous cell carcinoma. Int. J. Cancer 138, 2952–2962.
Rettig, E.M., D'Souza, G., 2015. Epidemiology of head and neck cancer. Surg. Oncol. Clin. N. Am. 24, 379–396.
Rodriguez-Perea, A.L., Arcia, E.D., Rueda, C.M., Velilla, P.A., 2016. Phenotypical characterization of regulatory T cells in humans and rodents. Clin. Exp. Immunol. 185, 281–291.
Schwartz, M., Zhang, Y., Rosenblatt, J.D., 2016. B cell regulation of the anti-tumor response and role in carcinogenesis. J. Immunother. Cancer 4, 40.
Shalapour, S., Font-Burgada, J., Di Caro, G., Zhong, Z., Sanchez-Lopez, E., Dhar, D., Willimsky, G., Ammirante, M., Strasner, A., Hansel, D.E., Jamieson, C., Kane, C.J., Klatte, T., Birner, P., Kenner, L., Karin, M., 2015. Immunosuppressive plasma cells impede T-cell-dependent immunogenic chemotherapy. Nature 521, 94–98.
Shang, B., Liu, Y., Jiang, S.J., Liu, Y., 2015. Prognostic value of tumor-infiltrating FoxP3+ regulatory T cells in cancers: a systematic review and meta-analysis. Sci. Rep. 5, 15179.
Skorupski, K.A., O'Brien, T.G., Guerrero, T., Rodriguez, C.O., Burns, M.R., 2011. Phase I/II clinical trial of 2-difluoromethyl-ornithine (DFMO) and a novel polyamine transport inhibitor (MQT 1426) for feline oral squamous cell carcinoma. Vet. Comp. Oncol. 9, 275–282.
Strauss, L., Bergmann, C., Gooding, W., Johnson, J.T., Whiteside, T.L., 2007. The frequency and suppressor function of CD4+CD25highFoxp3+ T cells in the circulation of patients with squamous cell carcinoma of the head and neck. Clin. Cancer Res. 13, 6301–6311.
Supsavhad, W., Dirksen, W.P., Martin, C.K., Rosol, T.J., 2016. Animal models of head and neck squamous cell carcinoma. Vet. J. 210, 7–16.
Tsai, H.F., Hsu, P.N., 2017. Cancer immunotherapy by targeting immune checkpoints: mechanism of T cell dysfunction in cancer immunity and new therapeutic targets. J. Biomed. Sci. 24, 35.
Wallis, S.P., Stafford, N.D., Greenman, J., 2015. Clinical relevance of immune parameters in the tumor microenvironment of head and neck cancers. Head Neck 37, 449–459.
Wypij, J.M., 2013. A naturally occurring feline model of head and neck squamous cell carcinoma. Patholog. Res. Int. 2013, 502197.
Yang, B., Jia, L., Guo, Q., Ren, H., Hu, Y., Xie, T., 2016. Clinicopathological and prognostic significance of cyclooxygenase-2 expression in head and neck cancer: a meta-analysis. Oncotarget 7, 47265–47277.
Yoshikawa, H., Ehrhart, E.J., Charles, J.B., Thamm, D.H., Larue, S.M., 2012. Immunohistochemical characterization of feline oral squamous cell carcinoma. Am. J. Vet. Res. 73, 1801–1806.
Zelenay, S., Lopes-Carvalho, T., Caramalho, I., Moraes-Fontes, M.F., Rebelo, M., Demengeot, J., 2005. Foxp3+ CD25- CD4 T cells constitute a reservoir of committed regulatory cells that regain CD25 expression upon homeostatic expansion. Proc. Natl. Acad. Sci. U. S. A. 102, 4091–4096.